Peer-reviewed version available at *Materials* **2018**, *11*, 1673; doi:10.3390/ma11091673

Article

Fabrication and Characterization of Electrospun PHA/Graphene Silver Nano-Composite Scaffold for Antibacterial Application

Abdul Mukheem [1,*], Kasturi Muthoosamy [2], Sivakumar Manickam [2], Kumar Sudesh [3], Syed Shahabuddin [4,*], Saidur Rahman [4,5], N. Akbar [6] and Nanthini Sridewi [1,*]

[1] Department of Maritime Science and Technology Faculty of Science and Defence Technology, National Defence University of Malaysia. nanthini@upnm.edu.my

[2] Department of Chemical and Nanopharmaceutical Process Engineering, Faculty of Engineering, University of Nottingham Malaysia Campus. sivakumar.manickam@nottingham.edu.my

[3] Applied Microbiology and Ecobiomaterial Research Laboratory, School of Biological Sciences, Universiti Sains Malaysia. ksudesh@usm.my

[4] Research Centre for Nano-Materials and Energy Technology (RCNMET), School of Science and Technology, Sunway University, 47500 Selangor Darul Ehsan, Malaysia. syedshahab.hyd@gmail.com

[5] Department of Engineering, Lancaster University, LA1 4YW, United Kingdom. saidur@sunway.edu.my

[6] Department of Biological Sciences, School of Science and Technology, Sunway University, Malaysia. noormicrobiologist555@gmail.com

* Correspondence: mukheembio@gmail.com; syedshahab.hyd@gmail.com; nanthini@upnm.edu.my Tel.: +60-124-675-320

Abstract: Many wounds are unresponsive to current available treatment techniques and therefore there is an immense need to explore suitable materials including biomaterials, which are being considered as the crucial factor to accelerate the healing cascade. In this study, we fabricated polyhydroxyalkanoate based antibacterial mats via electrospun technique. One-pot green synthesized graphene decorated silver nanoparticles (GAg) were incorporated into the fibres of poly-3 hydroxybutarate-*co*-12 mol% hydroxyhexanoate (P3HB-*co*-12mol% HHx), a co-polymer of polyhydroxyalkanoate (PHA) family which is highly biocompatible, biodegradable and flexible in nature. The synthesised PHA/GAg biomaterial was characterized by field emission scanning electron microscopy (FESEM), elemental mapping, thermogravimetric analysis (TGA), UV-visible spectroscopy (UV-vis) and Fourier transform infrared spectroscopy (FTIR). *In-vitro* antibacterial analysis were performed to investigate the efficacy of PHA/GAg against gram positive *Staphylococcus aureus* (*S.aureus*) strain 12600 ATCC and gram negative *Escherichia coli* (*E.coli*) strain 8739 ATCC. The results indicated that the PHA/GAg demonstrated significant reduction of *Staphylococcus aureus* (*S.aureus* strain 12600 ATCC) and *Escherichia coli* (*E.coli* strain 8739 ATCC) as compared to bare PHA or PHA-rGO in 2 hours of time. The P value ($P < 0.05$) was obtained by using 2 sample *T*-test distribution.

Keywords: graphene; silver nanoparticles; PHA; electrospun biomaterial; antibacterial.

1. Introduction

Skin is one of the largest organ of the human body with profuse functionalities. The key function of the skin is to protect the human body from the various environmental hazards such as shielding against exposure to harmful chemicals, ultraviolet radiation and pathogenic organisms.

Damage to the skin is a common phenomenon and a unique challenge, as wound therapeutic is a complex process which requires considerable amount of time. Many wounds are unresponsive to the existing treatment thereby making these wounds as the cumulative threat to public health and the economy [1]. Currently, the drug resistance has shown the common occurrence among many bacteria's including *E.coli* and *S.aureus* species (super-bugs) [2,3]. Thus, there is an urgent need to identify biogenic effective nanomaterials with broad spectrum antibacterial properties to tackle the current problem of wound healing.

Many efforts are being made for better wound management by making the use of extensive biocompatible nanomaterials. The ideal biomaterial for wound dressing must be possessing properties such as biocompatibility, gaseous exchange, flexibility, biodegradability, safeguard to prevent the bacterial infection and remove excess exudates [4,5]. Some of the commonly used polymers in medicine namely silicones, have been suspected to cause cancer and thus must be replaced by some biocompatible polymers [6]. Among various available biogenic polymers, polyhydroxyalkanoate (PHA) is a biopolymer produced by various bacterial cells under imbalanced growth condition [7]. General structure of PHA has been depicted in figure 1. PHA is vastly investigated biopolymer and is well known for its excellent properties namely nontoxic nature, biocompatibility and biodegradability [8-10]. The degradation product of poly 3-hydroxybutrate (P3HB) is a common metabolite in all higher living beings which is an important aspect of PHA [11]. In recent years, poly 4-hydroxybutyrate (P4HB), poly 3-hydroxybutrate and copolymer poly 3-hydroxybutyrate-co-3-hydroxyhexanoate (PHBHHx) [12,13] has been widely used in the field of medicine to develop the biologically significant devices including sutures, cardiovascular scaffolds, orthopedic scaffolds, adhesion barriers, guided tissue repair, nerve guides, tendon repair and wound dressings [14-19]. The versatile structure of PHA could simply be modified through physical blending and chemical alteration to improve its efficacy for medicinal use. However, reinforcement of nanoparticles and nanocomposite feasibly enhance the resulting scaffold with multiple functionalities for efficient therapeutic and tissue engineering applications.

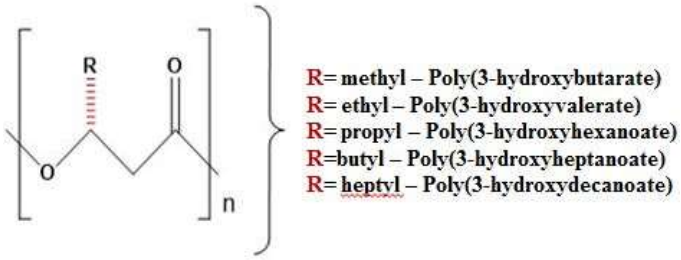

Figure 1. General Structure of Polyhydroxyalkanoate.

Graphene is a two-dimensional sheet of sp2-hybridized carbon atoms densely packed into a honeycomb lattice [20]. Graphene and its derivatives have received much attention for its excellent physicochemical properties like good thermal and optical properties, high surface area to volume ratio, high strength, good elastic properties, ease of functionalization and chemical inertness [21-23]. Due to these distinctive properties, graphene is often used as a suitable matrix for designing biomedical devices with feasible substances includes polymers and nanoparticles. In the past decade, graphene has been widely investigated for its antibacterial, antiplatelet, anticancer and biosensor activities [24-26]. rGO exerts its antibacterial property through oxidizing agent glutathione that serve as redox state mediator in bacteria and also disrupt bacterial cell membrane upon direct contact [27]. Apart from antibacterial application, graphene have been used in various applications in the field of sensors, supercapacitors, energy storage devices, fuel cells and high-strength materials [28-30] . Several salient features of graphene make it a potential candidate for biomedical use. One of the most attractive feature of graphene is high surface area to volume ratio (2630 m^2g^{-1}), which makes it a suitable candidate for nucleation of various nanoparticles. To improve physicochemical

properties of rGO, nanoparticles have been incorporated within its matrix by the physical, chemical and biological approaches. In recent years, rGO based nanocomposites have been reported with metal nanoparticles specifically with gold, silver and platinum [31]. Nanoparticles or nanocomposites are now considered as a feasible alternative to antibiotic and perhaps have a high potential to solve the emergence of bacterial multidrug resistance [32].

Among the noble metals, silver nanoparticles (Ag-NPs) have been extensively investigated due to its ease synthesis and unique properties including antiseptic, antibacterial, low cytotoxicity, high electrical and thermal conductivity [33,34]. Ag-NPs find application in diverse fields like optical sensors, textile engineering, electronics, bactericidal agent, dental resin composites, coating of medical devices, water filters, air sanitizer sprays, pillows, respirators, wet wipes, detergents, toothpastes, bone cement, wound dressing and therapeutic agent. Sanitization through Ag-NPs have been reported to be extremely toxic to bacterial cells depending on its size and distribution [35,36]. The modes of antibacterial action of silver nanoparticles are, it interacts with the sulfate group on bacterial cell surface which blocks some enzymes responsible for energy metabolism and electrolyte transport. Thus the oxidation stress damage the membrane, lack of enzyme suffocates and enforce bactericidal phenomena [37]. However, the size related surface energy stimulates the agglomeration of Ag-NPs that perhaps loses its efficacy of antibacterial properties. To minimize Ag-NPs agglomeration, rGO high surface area is an excellent supporting matrix [38]. The synergistic antibacterial effect of rGO and Ag-NPs nanocomposite (GAg) makes it an ideal antibacterial agent with dual killing effect [39-41]. Numerous physical and chemical protocols have been reported in various literatures to synthesize graphene and silver nanoparticles. However, these methods are expensive or use toxic substances which make them non compatible for medical application. The more suitable way to synthesize biocompatible and less toxic rGO and Ag-NPs composite is the use of green materials such as plant extract [38,42]. Nanomaterials synthesized using green techniques are less toxic, eco-friendly and compatible for biomedical applications [43]. Recently, many techniques have been reported using plant and fungal extracts for the biosynthesis of GAg nanocomposite [44]. In this investigation, GAg nanocomposite is synthesized biogenically using cheaply available *Ganoderma lucidium* (G.L.) extract as a strong reducing agent [45]. The rich content of polysaccharide (glucans) in G.L. extract assists the reduction of graphene oxide (GO) and silver nitrate in a single reaction to produce GAg nanocomposite. Electrospinning has gained lots of scientific consideration owing to its ability to produce biomedical attractive materials within nanoscale regime, since, the as-spun fibers mimic the nanoscale properties of native extracellular matrix. Electrospun fibrous porous biomaterial has been investigated as promising tissue engineering, antibacterial and wound dressing scaffolds [8,9,46].

In the present study, we intended to integrate the broad spectrum antimicrobial activity of GAg nanocomposite with the biocompatibility of P3HB-co-12mol%HHx (hereafter mentioned as PHA) through electrospun technique. The outstanding properties of PHA comprising biocompatible nature, enhanced biodegradability in set time frames and flexibility are the suitable features to support wound healing. Alongside, it is assumed in the GAg nanocomposite, that Ag-NPs loaded onto rGO will allow stabilization and curb agglomeration of the nanoparticles. The narrow size distribution of Ag-NPs on the high surface area of rGO maximizes the direct contact of nanoparticles with bacterial cells which improves the bactericidal activity. To the best of our knowledge, there is no report on the application of as-spun PHA/GAg nanocomposite mats for antibacterial studies. It is hypothesized that, PHA/GAg scaffold exhibit dual bactericidal properties. The antimicrobial activities of the as-spun mats have tested against *Escherichia coli* and *Staphylococcus aureus*.

2. Materials and Methods

Graphite powder was received from Asbury Graphite Mill Inc., Asbury, USA. Silver nitrate ($AgNO_3$) and sodium hydroxide (NaOH) were obtained from Sigma-Aldrich, USA. Chloroform ($CHCl_3$) and dimethylformamide (DMF) solvents of analytical grade were purchased from

Sigma-Aldrich, Malaysia. *Ganoderma lucidium* powder was received from Ganofarm Sdn. Bhd., Port Dickson, Malaysia. P3HB-*co*-12mol% HHx (350,000 Da) was porvided by KANEKA corporation, Japan. Ultra pure deionised water was obtained from Milli-Q plus system, EMD millipore, USA. Electrospinning of scaffold was carried out using Esprayer ES-2000, Fuence Co. Ltd., Japan. Stationary phase bacterial strains. *S.aureus* (12600 ATCC) and *E.coli* (8739 ATCC) were used for antibacterial studies. To prepare stationary-phase cultures, diluted cultures were grown for 16 hours prior to testing.

2.2 Preparation of Reducing Agent, G.L. Extract

In a 250ml of conical flask, 1 gram of G.L. mushroom powder and 100 mL Milli-Q grade water was added. This mixture was placed in a hot water bath for 3 hours at 85^{0}C and then is cool down at room temperature. The solution was transferred to 50ml eppendrof tubes. To confiscate the suspended particles of G.L. mushroom, the reacted solution was centrifuged at 10,000 rpm for 15 minutes. The clear supernatant was collected carefully and used as reducing agent diectly or can be stored at 4^{0}C for further use. Figure 2 provides the pictorial illustration of the preparation of G.L. extract.

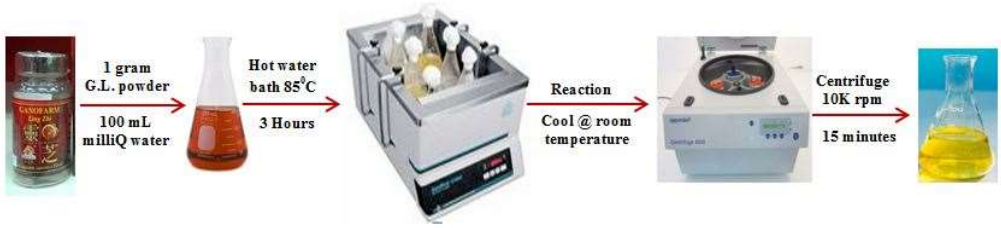

Figure 2. Shecmatic illustration of preparing Ganoderma lucidium extract.

2.3 Synthesis of GAg Nanocomposite

GAg was synthesized using GO (graphite oxide) (prepared via modified Hummers method using flake graphite), AgNO3 and G.L. mushroom extract. The pH of GO solution (0.1 mg/mL) was adjusted to 7 by using NaOH. For synthesizing GAg nanocomposite, to the 25 mL of 0.1 mg/mL GO solution, 10 mM AgNO3 was added dropwise in a 250 mL conical flask containing 25 mL of G.L. extract. The mixture was then placed in a preheated rotary water bath, maintained at the speed of 120 rpm at 850 C for 16 hours. The resulting solution was then allowed to cool at room temperature and then transferred to 50ml eppendrof tubes for centrifugation. The reaction mixture was centrifuged at 10,000 rpm for 20 minutes and the supernant was discarded. The resulting solid residue was again dispersed in DI water and washed through centrifuge to remove all the residuals of G.L. extract. This step was repeated for 5 times in order to obtain pure GAg nanocomposite. Since the G.L. extract is water soluble, it is easy to remove entirely from the reaction solution with simply water washing technique. Finally, the resultant GAg nanocomposite pallet was gently re-dispersed in milli-Q water for further use. Figure 3 shows the schematic description of GAg nanocomposite.

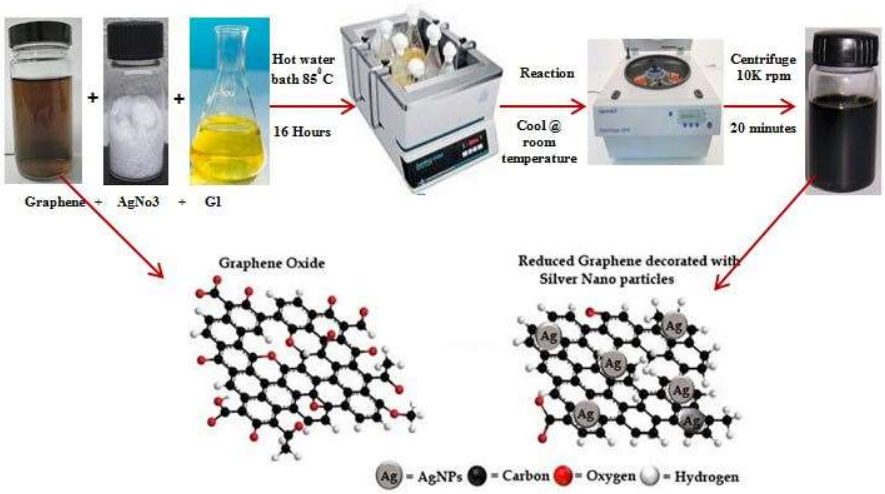

Figure 3. Green synthesis of GAg nanocomposite.

2.4 Fabrication of Electrospun Scaffold (PHA/GAg)

Electrospinning precursor solution was prepared using the organic solvents $CHCl_3$ and DMF (8:2 ratio) [47], containing 5 ml of 3% (w/v) of P3HB-*co*-12 mol% HHx and 15 microL of GAg. Precursor solution was subjected to magnetic stirring for 48 hours at room temperature followed by 2 hours heat treatment at 55^{0}C to dissolve PHA completely. It was then sonicated in water bath for 5 mins prior to electrospinning to have even distribution of GAg in PHA solution. Similar steps were applied to make precursor solution of rGO (reduced graphene oxide) and control (PHA alone). Esprayer ES-2000 (Fuence, Co. Ltd., Japan) was used to electrospun the nanocomposite mats. PHA/GAg mats (Figure 4) were formed at an applied voltage of 25kV and extrusion rate of 40 µL/min at the fixed distance of 20 cm from the needle tip to copper plate collector. Total 5 mL of PHA/GAg precursor solution was fed to electrospun to obtained a scaffold of 4x4 cm. The obtained product of PHA/GAg scaffold was then vacuum dried for 24 hours to eliminate any residuals of $CHCL_3$ and DMF.

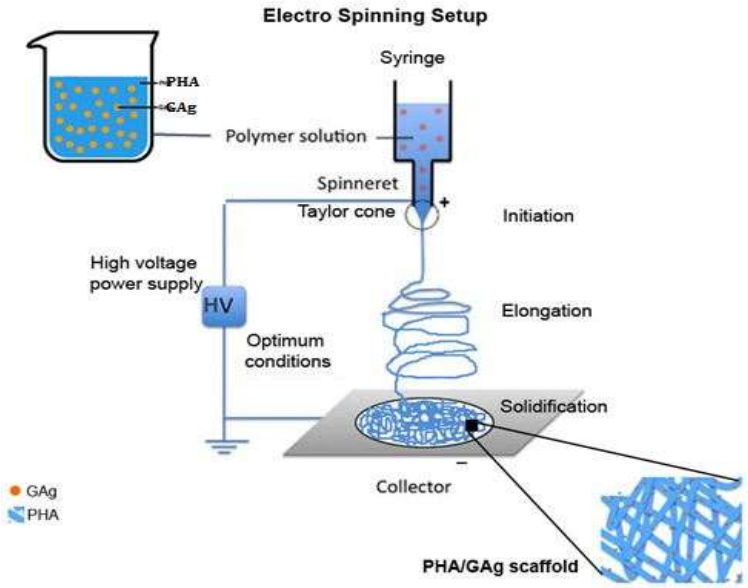

Figure 4. Schematic diagram of electro spinning PHA/GAg scaffold.

2.5 Antibacterial Culture Preparation

PHA/GAg, rGO and control with the disc size 0.6mm was tested against *S.aureus* (12600 ATCC) and *E.coli* (8739 ATCC) as the model organisms by using time kill test technique. Diluted cultures were grown upto 6 hours in a 100ml of nutrient broth prior to testing. Prepared precursor broth containing test organisms were equally transferred to sterile bijous bottles of size 15 ml. Moreover, the discs of test scaffolds (PHA/GAg, PHA/rGO and PHA) was exposed to UV for 30 minutes and then placed aseptically in the precursor broth aliquoted into the bottles. The aliquot in control bottle was treated with PHA disc alone as a negative control. In the following analysis, gentamicin was used as a positive control for 100% kill. The bottles were incubated at 37°C in a shaker incubator at 150 rpm. The samples were collected at different time intervals at 0, 2, 4, 6 and 24 h and then serially diluted until optimized working dilution. Finally, 100µL precursor broth sample treated with as-spun nanocomposite mats was aspirated and dispensed onto the freshly prepared nutrient agar plate with 2 duplicates each followed by the spread plate technique and incubated at 37°C for overnight to obtain the antibacterial activity of as-spun PHA/GAg and PHA/rGO scaffolds.

3. Characterization

The surface structure and morphology of the PHA/GAg mats were studied using FESEM (Hitachi nanoDUE'T NB5000 USA). The rGO was examined using ultraviolet–visible (UV–Vis) spectrum at predetermined time intervals using Lambda 35 Spectrophotometer (Perkin Elmer, Waltham, MA, USA). The particle size and stability were studied using zetasizer Nano ZS (Malvern Instruments, Malvern, UK). Ultrasonication was employed by using a Cole Parmer dip-stick sonicator (20 kHz ±5 kHz), using tapered microtip of 3 mm, with an amplitude of 44%, prior to zetasizer analysis. FTIR spectra of the PHA/GAg were obtained using Spectrum RX1 (Perkin Elmer) in the frequency range of 4,000–400 cm^{-1}. Thermo gravimetric (TGA) was performed by heating the samples from 25°C to 1,000°C at the heating rate of 5°C/min, under a nitrogen flow (50 mL/min) using a TGA/differential scanning calorimetry 1, Stare System (Mettler Toledo Inc., OH, USA).

3. Results

4.1 FESEM and Elemental Analysis

The surface morphology of the synthesised material was comprehensively analysed by FESEM technique. Figure 5 represents the FESEM micrographs of rGO, GAg and PHA/GAg electrospun mats. As evident from figure 5a, rGO exhibits transparent rippled silk-like waves and wrinkles type of morphology. Deletion of strain on the C-C bond in the epoxy groups forms the wrinkles [48]. The obtained result is in good agreement with many recent studies depicting graphene sheets obtained from GO, by various techniques, possessing to have curled morphologies consisting of thin, wrinkled, paper-like structures, with fewer layers and having larger specific surface areas than GO [49]. The FESEM micrograph of Ag-NPs reveals the formation of spherical particles within nano-range as depicted in figure 5b. The morphological analysis of GAg nanocomposite decorated on PHA fibres is illustrated by figure 5c. As apparent from figure 5c, there is a formation of porous mat like matrix with fibrous morphology indicating the formation of fibrous PHA/GAg nanocomposite.

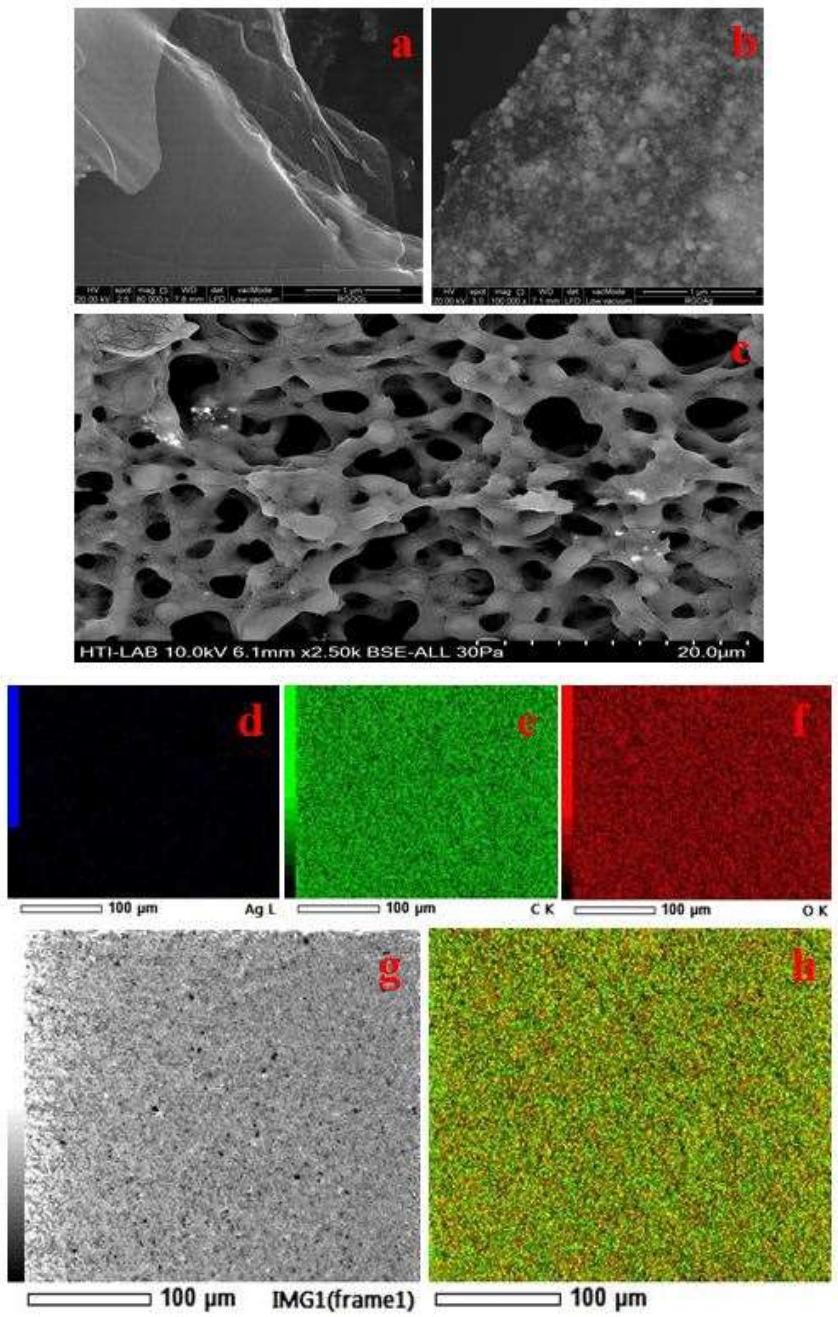

Figure 5. SEM images for the rGO (a), GAg (b) and PHA/GAg electrospun mats (c). Elemental mapping of sample PHA/GAg scaffold has shown in figure (d,e,f and h) respectively.

However, it is difficult to locate silver nanoparticles on the PHA/GAg nanocomposite since these particles are embedded deep within the polymer matrix and hard to visualise by FESEM analysis. Thus, elemental mapping appears to be the best technique to establish the uniform presence of Ag nanoparticles within the matrix of PHA polymer. Figure 5d,e,f,g and h represents the elemental mapping analysis of PHA/GAg nanocomposite which evidently reveals that Ag nanoparticles are homogeneously present within the matrix of the composite material along with carbon and oxygen.

4.2 UV-vis Analysis

Figure 6 displays the UV-vis diffuse reflectance spectrum for the Ag nanoparticles, rGO and PHA/GAg respectively. As evident from figure 6a, the UV-vis spectrum of Ag-NPs exhibit a distinct broad absorption peak at about 410 nm which is the characteristic peak for Ag and indicates the successful formation of Ag-NPs [50]. On the other hand, the UV-vis spectrum of rGO (Figure 6b) demonstrates a broad band at 260 nm which can be attributed to the conjugated sp^2 carbon network in rGO and is a characteristic of rGO [51]. Since, no significance plasmon peak appears at 300 nm in the spectrum of rGO, suggesting the removal of oxygen groups and thereby confirming the successful reduction of GO to rGO [52]. Moreover, the characteristic peak of GO appears at 230 nm which is absent in the spectrum of rGO, thereby confirming the formation of rGO. As apparent from figure 6c, the UV- vis spectrum of GAg reveals the presence of the characteristic peaks for both Ag and rGO thereby demonstrating the successful synthesis of Ag nanoparticles decorated rGO.

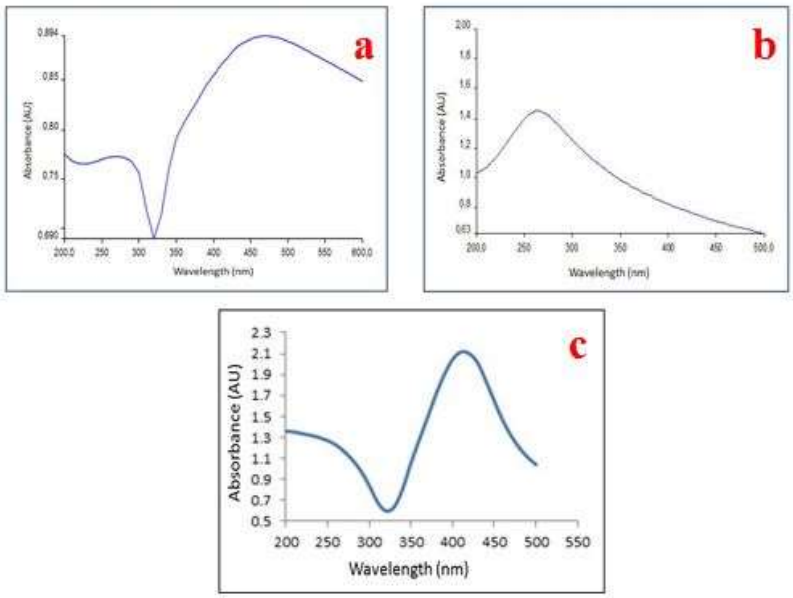

Figure 6. UV-vis spectra obtained after the green synthesis of Ag-NPs (a), rGO (b) and GAg (c).

4.3 Particle Size Analysis

Furthermore the particle size distribution of GAg was determined by DLS (Dynamic Light Scattering) analysis which is the most valuable and useful technique to assess particle size and size distribution of any nanomaterial in solution [53]. The results of DLS demonstrated that the size distribution of Ag-NPs within GAg was found to be ranging from 10 to 80 nm in diameter. The z-average diameter noted for Ag-NPs was found to be 66.52 nm (Figure 7). DLS technique can be used for the study of rGO based composites, but the dimensions of rGO sheets and GO-based nanocomposites determined by this technique does not represent the real particle size [54]. Though DLS is appropriate for spherical particles rather than planar sheets like rGO, it serves to indicate whether uniformly sized dispersion of graphene was produced. The particle size distribution in the case of GAg as detected by DLS exhibited the presence particles of around 30 to 120 nm which may be attributed to the agglomeration of Ag-NPs or rGO flakes.

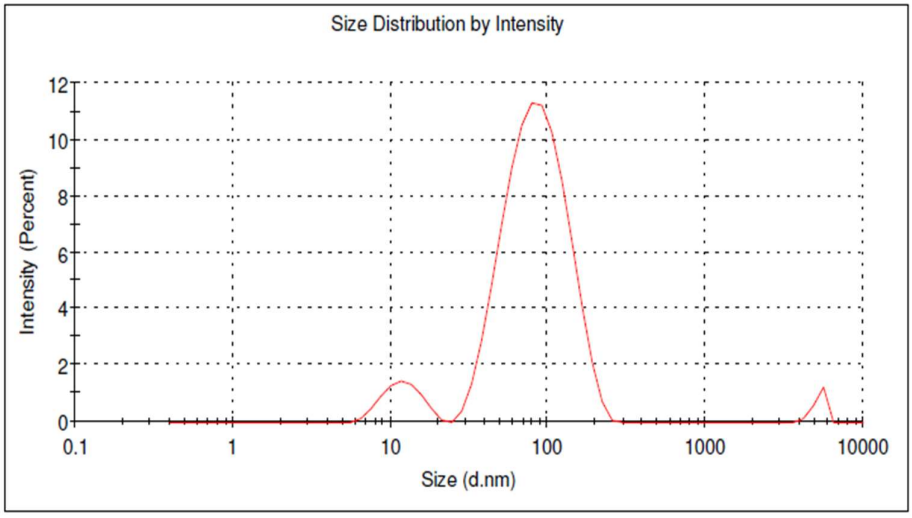

Figure 7. Dynamic light scatter of GAg nanocomposite.

4.4 FTIR Analysis

The FTIR spectra of rGO nanoflakes, GAg are shown in figure 8a and for PHA embedded GAg nanocomposites spectra is shown in figure 8b. The IR band appears at approximately 3414, 1725, 1626, 1245 and 1060 cm^{-1} of rGO are assigned to –OH stretching vibrations, C=O stretching of Carboxylic groups, O H deformations of the C-OH groups, epoxy symmetrical ring deformation vibrations and C-O stretching vibrations, respectively [55]. The peaks at 1060 cm^{-1} (C-O stretching vibrations), 1245 cm−1(C-OH stretching vibration) and 1725 cm^{-1} (C=O stretching vibration) were become less intense; which suggests the reduction of graphene. The peaks in between 2924 cm^{-1} to 3400 cm^{-1} of silver were assigned to the stretching vibrations of primary and secondary amines, while their corresponding bending vibrations were seen at 1383 cm^{-1} and 1636 cm^{-1} respectively [56]. The wave number positioned around 1700 cm^{-1} was attributed to the stretching vibration of the C=O group (ester carbonyl) in the PHA. Associated bands of the C-O-C groups appeared in the spectral region of 1150 to 1300 cm^{-1}. P3HB-*co*-HHx had the strongest methylene -C-H- vibrations at around 2933 cm^{-1}. And the wavenumbers at 3436 cm^{-1} is assigned to the OH vibration in carboxyl group of P(3HB-co-3HHx) [57,58]. The overall observation of FTIR band confirms the successful formation of PHA/GAg composite mat.

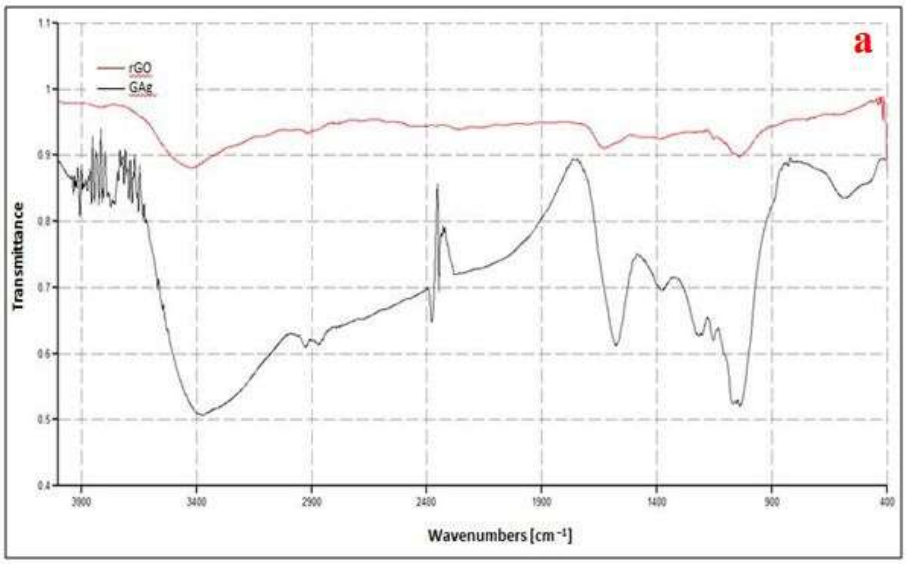

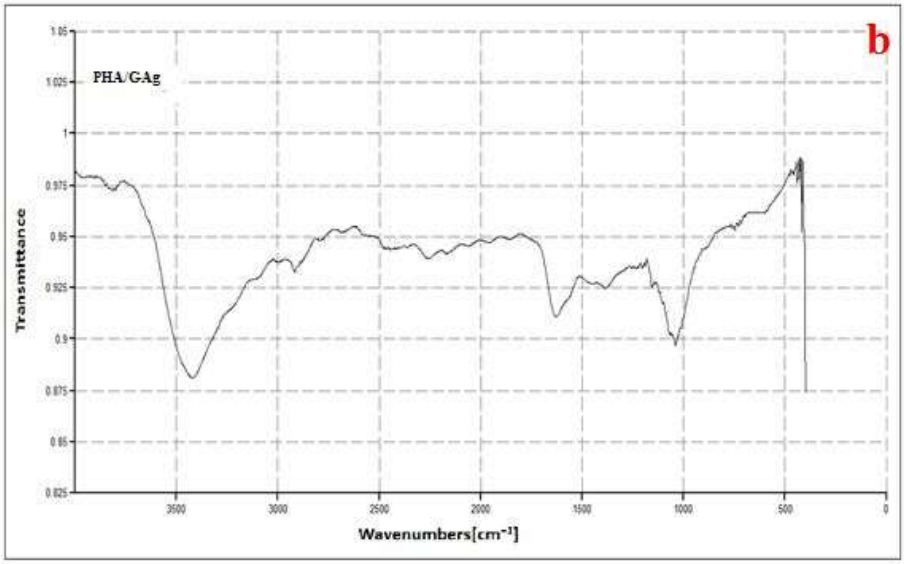

Figure 8. FTIR spectra of rGO, GAg (a) and PHA/GAg (b) nanocomposites.

4.5 Thermal Analysis

Thermal stability of GAg and rGO were analyzed using TGA. Figure 9 exhibits TGA curves of rGO and GAg nanocomposite under nitrogen atmosphere. The decomposition of rGO and GAg begins with moderate weight loss at around 100°C to 250 °C which is probably due to removal of water molecules, oxygen functional group and residues. The maximum weight loss was observed from 250°C to 400°C for both rGO (38%) and GAg (28%) which may be due to the loss of left over oxygen functional group and bulk pyrolysis of the carbon skeleton. TGA curves of rGO and GAg exhibit a slight mass loss at temperature around 600°C, which suggests that the enhancement of thermal stability is achieved after the oxygen-containing functional groups were removed during reduction [59,60]. TGA results of GAg showed better thermal stability as compare to rGO alone. GAg has less oxygen groups and contains AgNPs which can affect the thermal stability of graphene, suggesting strong interaction between rGO and Ag.

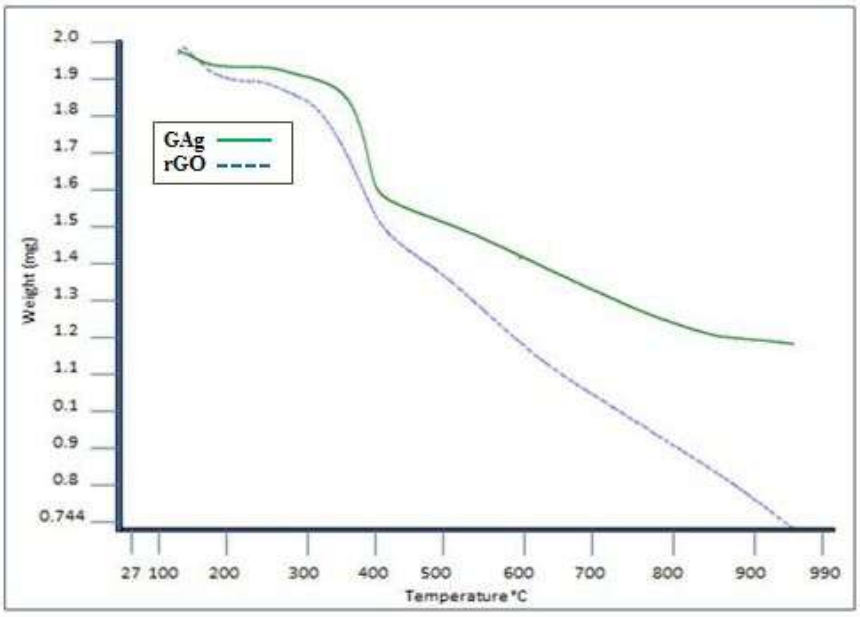

Figure 9. TGA spectra of rGO and GAg nanocomposites.

4.6 Antibacterial Analysis

Antibacterial activity of as-spun nanocomposite was obtained against model organism *E.coli* and *S.aureus* through time kill method. Sterile bottles containing 0.6mm discs of PHA, PHA/rGO and PHA/GAg nanocomposite were aliquotted with 5mL of culture broth of each test organism separately. Gentamicin was used as a positive control which is a broad spectrum antibiotic with effective bactericidal activities. Its mode of action includes inhibition of bacterial protein synthesis by binding to 30S ribosomes inside the bacteria cell. The aliquot in control bottle was treated with PHA disc alone as a negative control. All bottles were agitated at 150 rpm in shaker incubator at the temperature of 37°C. After the set time intervals, 100 µL culture broth was aspirated from all the samples and dispensed onto the freshly prepared nutrient agar plates with 3 replicate of each sample followed by the spread plate technique under sterile condition and incubated at 37°C for overnight (14 hours).

The antibacterial activity of the as-spun nanocomposite was evaluated at different time intervals. In the first 2 and 4 hours of time interval the bactericidal activity of the tested samples against *E.coli* and *S.aureus* was highly significant with respective to 6, 24 hours samples. Moreover, upto 24 hours, PHA/rGO and PHA/GAg nanocomposite has shown significant reduction of bacterial cells in comparison with negative control. Significant, CFU percent inhibition was shown by *E.coli* inoculated with different test nanocomposite. The P value ($P < 0.05$) was obtained by using 2 sample *T*-test distribution, (*) is <0.05; (**) is <0.01; and (***) is <0.001 (Figure 10a). Similarly, *S.aureus* has also shown significant, CFU percent inhibition towards the tested nanocomposite ($P < 0.05$ using 2 sample *T*-test distribution (*) is <0.05; (**) is <0.01; and (***) is <0.001) (Figure 10b). These statistical analyses were further supported in table 1.

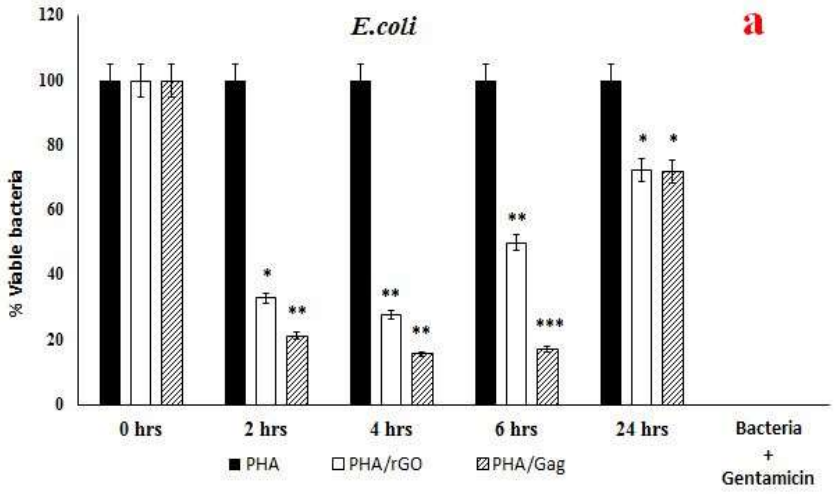

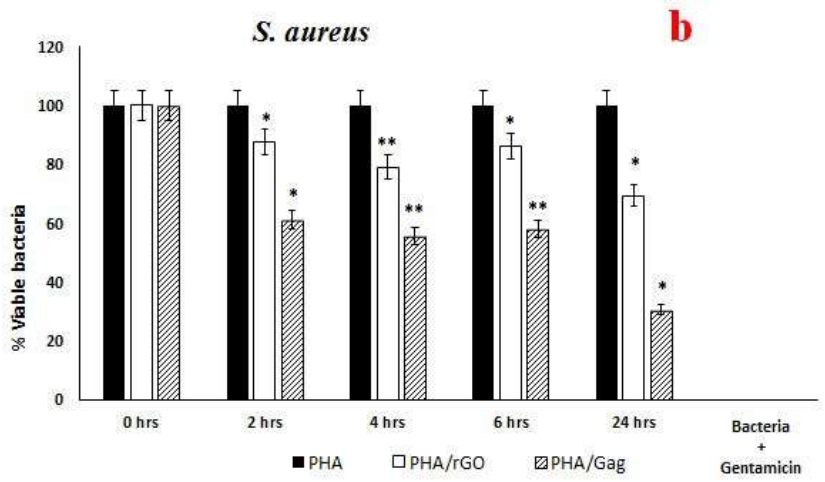

Figure 10. Bactericidal activity of PHA, PHA/rGO and PHA/GAg against test organism. PHA/rGO and PHA/GAg showed significant (P value < 0.05) bactericidal effects towards *E.coli* (a) and *S.aureus* (b). P values were determined using two sample *T*-test distribution, (*) is <0.05; (**) is <0.01; and (***) is <0.001.

Table 1. Representation of PHA, PHA/rGO and PHA/GAg scaffolds antibacterial activity against *E.coli* and *S.aureus*

Test Samples	Antibacterial activity against *E.coli*	Antibacterial activity against *S.aureus*
PHA	-	-
PHA/rGO	+	+
PHA/GAg	+	+
Gentamicin	+	+

Herein the 4 hours bactericidal activity of PHA/GAg against *E.coli* has shown (Figure S1) highly significant activity compared with the negative control and less significant as compared to PHA/rGO. Whereas, *S.aureus* treated with PHA/GAg demonstrated significant bactericidal activity (Figure S2) in comparison of PHA/rGO and negative control. Significant bacterial inhibition was obtained upto 4 hours of incubation and thereafter gradual decrease was observed until 24 hours in the test nanocomposites compare to control. Biogenically as-spun nanocomposites have shown less bactericidal activity with respect to commercial gentamicin.

5. Conclusions / Discussion

In conclusion, PHA/rGO and PHA/GAg nanocomposites were successfully fabricated using electrospinning technique. Through the electrospinning procedure, GAg nanocomposite have been eventually distributed and embedded on the as-spun fibres of PHA, which makes PHA/GAg an effective antibacterial scaffold. The obtained scaffolds were vaccum dried for 48 hours to remove the residuals of chloroform and DMF. Then the resultant scaffolds were tested for their antibacterial properties against test organisms. Significant bactericidal activity was observed in first 2 and 4 hours of time interval compared to 6 and 24 hours. It is hypothesized that, silver ions were actively released into the inoculum for first 4 hours of time interval followed by gradual release until 24 hours. *E.coli* has shown more sensitivity towards the tested nanocomposites as compared to *S.aureus*. PHA/GAg has shown significant bactericidal activity in compare to PHA/rGO and negative control. The antibacterial activity was recorded upto 24 hours of incubation, which is an important factor for

an effective wound dressing. Therefore, as-spun PHA/GAg nanocomposite may be feasibly efficient in the treatment of chronic wound and sanitizing applications.

Supplementary Materials: Figure S1: At the time intravel of 4 h bactericidal activity of PHA, PHA/rGO and PHA/GAg against E.coli was evaluated. Significant decrease is observed in the CFU which demonstrates the bactericidal activity of PHA/rGO and PHA/GAg compare to PHA alone. PHA/GAg is consider very effective with its dual mode of action (reduced graphene and silver nanoparticles) towards the E.coli and is highly significant. Positive control data has not presented here. Figure S2: The antibacterial activity after 4 h time intraval, was evaluated for PHA, PHA/rGO and PHA/GAg against S.aureus. Significant decrease is observed in the CFU which demonstrates the bactericidal activity of PHA/rGO and PHA/GAg compare to PHA alone. PHA/rGO and PHA/GAg has shown less reduction compare to E.coli. Positive control data has not presented here.

Author Contributions: Conceptualization: Nanthini Sridewi. and Abdul Mukheem.; Methodology: Nanthini Sridewi., Kasturi Muthoosamy. and Abdul Mukheem.; Software: N. Akbar.; Validation: Nanthini Sridewi. and Syed Shahabuddin.; Formal Analysis: Abdul Mukheem.; Investigation: Abdul Mukheem.; Resources: Nanthini Sridewi., Sivakumar Manickam., Kumar Sudesh. and Saidur Rahman; Data Curation: Abdul Mukheem.; Writing-Original Draft Preparation: Abdul Mukheem.; Writing-Review & Editing: Nanthini Sridewi. and Syed Shahabuddin.; Visualization: Abdul Mukheem. and Syed Shahabuddin.; Supervision: Syed Shahabuddin and Nanthini Sridewi; Project Administration: Nanthini Sridewi.; Funding Acquisition: Nanthini Sridewi.

Funding: This research was funded by [Ministry of Science, Technology and Innovation (MOSTI), Malaysia] grant number [2014/03-01-19-SF0127].

Acknowledgments: The authors would like to thank the Ministry of Science, Technology and Innovation (MOSTI), Malaysia, for the research facilities and financial support through research grant ScienceFund award number 2014/03-01-19-SF0127.

Conflicts of Interest: The authors declare no conflict of interest.

References

1. Walker, B.; Barrett, S.; Polasky, S.; Galaz, V.; Folke, C.; Engström, G.; Ackerman, F.; Arrow, K.; Carpenter, S.; Chopra, K. Looming global-scale failures and missing institutions. *Science* **2009**, *325*, 1345-1346.
2. Organization, W.H. *Antimicrobial resistance: Global report on surveillance*. World Health Organization: 2014.
3. Demain, A.L. Antibiotics: Natural products essential to human health. *Medicinal Res. Rev.* **2009**, *29*, 821-842.
4. Jayakumar, R.; Prabaharan, M.; Kumar, P.S.; Nair, S.; Tamura, H. Biomaterials based on chitin and chitosan in wound dressing applications. *Biotech. Adv.* **2011**, *29*, 322-337.
5. Unnithan, A.R.; Gnanasekaran, G.; Sathishkumar, Y.; Lee, Y.S.; Kim, C.S. Electrospun antibacterial polyurethane–cellulose acetate–zein composite mats for wound dressing. *Carbohyd. polym.* **2014**, *102*, 884-892.
6. Cammas, S.; Bear, M.-M.; Moine, L.; Escalup, R.; Ponchel, G.; Kataoka, K.; Guérin, P. Polymers of malic acid and 3-alkylmalic acid as synthetic phas in the design of biocompatible hydrolyzable devices. *Int. J. Bio. Macromolec.* **1999**, *25*, 273-282.
7. Sudesh, K.; Abe, H.; Doi, Y. Synthesis, structure and properties of polyhydroxyalkanoates: Biological polyesters. *Prog. Polym. Sci.* **2000**, *25*, 1503-1555.
8. Valappil, S.P.; Misra, S.K.; Boccaccini, A.R.; Roy, I. Biomedical applications of polyhydroxyalkanoates, an overview of animal testing and in vivo responses. *Expert Rev. Med. Devices* **2006**, *3*, 853-868.

9. Hazer, B. Amphiphilic poly (3-hydroxy alkanoate) s: Potential candidates for medical applications. *Int. J. Polym. Sci.* **2010**.
10. Yang, H.-X.; Sun, M.; Zhang, Y.; Zhou, P. Degradable phbhhx modified by the silk fibroin for the applications of cardiovascular tissue engineering. *ISRN Mater. Sci.* **2011**.
11. Doyle, V.; Pearson, R.; Lee, D.; Wolowacz, S.; Mc Taggart, S. An investigation of the growth of human dermal fibroblasts on poly-l-lactic acid in vitro. *J. Mater. Sci.: Mater.Med.***1996**, *7*, 381-385.
12. Wang, Y.-W.; Yang, F.; Wu, Q.; Cheng, Y.-c.; Peter, H.; Chen, J.; Chen, G.-Q. Effect of composition of poly (3-hydroxybutyrate-co-3-hydroxyhexanoate) on growth of fibroblast and osteoblast. *Biomaterials* **2005**, *26*, 755-761.
13. Chen, G.Q.; Wu, Q.; Wang, Y.W.; Zheng, Z. In *Application of microbial polyesters-polyhydroxyalkanoates as tissue engineering materials*, *Key Eng. Mater.* **2005**; Trans Tech Publ: pp 437-440.
14. You, M.; Peng, G.; Li, J.; Ma, P.; Wang, Z.; Shu, W.; Peng, S.; Chen, G.-Q. Chondrogenic differentiation of human bone marrow mesenchymal stem cells on polyhydroxyalkanoate (pha) scaffolds coated with pha granule binding protein phap fused with rgd peptide. *Biomaterials* **2011**, *32*, 2305-2313.
15. Misra, S.K.; Ansari, T.I.; Valappil, S.P.; Mohn, D.; Philip, S.E.; Stark, W.J.; Roy, I.; Knowles, J.C.; Salih, V.; Boccaccini, A.R. Poly (3-hydroxybutyrate) multifunctional composite scaffolds for tissue engineering applications. *Biomaterials* **2010**, *31*, 2806-2815.
16. Kurobe, H.; Maxfield, M.; Naito, Y.; Breuer, C.; Shinoka, T. Stem cells in tissue-engineered blood vessels for cardiac repair. *Cardi. Regene. Repair*, Elsevier: **2014**; pp 389-409.
17. Lu, X.-Y.; Ciraolo, E.; Stefenia, R.; Chen, G.-Q.; Zhang, Y.; Hirsch, E. Sustained release of pi3k inhibitor from pha nanoparticles and in vitro growth inhibition of cancer cell lines. *Appl. Microbio. Biotech.* **2011**, *89*, 1423-1433.
18. Xu, X.-Y.; Li, X.-T.; Peng, S.-W.; Xiao, J.-F.; Liu, C.; Fang, G.; Chen, K.C.; Chen, G.-Q. The behaviour of neural stem cells on polyhydroxyalkanoate nanofiber scaffolds. *Biomaterials* **2010**, *31*, 3967-3975.
19. Zonari, A.; Martins, T.M.; Paula, A.C.C.; Boeloni, J.N.; Novikoff, S.; Marques, A.P.; Correlo, V.M.; Reis, R.L.; Goes, A.M. Polyhydroxybutyrate-co-hydroxyvalerate structures loaded with adipose stem cells promote skin healing with reduced scarring. *Acta Biomaterialia* **2015**, *17*, 170-181.
20. Novoselov, K.S.; Geim, A.K.; Morozov, S.V.; Jiang, D.; Zhang, Y.; Dubonos, S.V.; Grigorieva, I.V.; Firsov, A.A. Electric field effect in atomically thin carbon films. *Science* **2004**, *306*, 666-669.
21. Suk, J.W.; Lee, W.H.; Lee, J.; Chou, H.; Piner, R.D.; Hao, Y.; Akinwande, D.; Ruoff, R.S. Enhancement of the electrical properties of graphene grown by chemical vapor deposition via controlling the effects of polymer residue. *Nano letters* **2013**, *13*, 1462-1467.
22. Lee, C.; Wei, X.; Kysar, J.W.; Hone, J. Measurement of the elastic properties and intrinsic strength of monolayer graphene. S*cience* **2008**, *321*, 385-388.
23. Loh, K.P.; Bao, Q.; Ang, P.K.; Yang, J. The chemistry of graphene. *J. Mater. Chem.* **2010**, *20*, 2277-2289.
24. Akhavan, O.; Ghaderi, E. Toxicity of graphene and graphene oxide nanowalls against bacteria. *ACS nano* **2010**, *4*, 5731-5736.
25. Zuchowska, A.; Chudy, M.; Dybko, A.; Brzózka, Z. Graphene as a new material in anticancer therapy-in vitro studies. *Sensors and Actuators B: Chemical* **2017**, *243*, 152-165.
26. Justino, C.I.; Gomes, A.R.; Freitas, A.C.; Duarte, A.C.; Rocha-Santos, T.A. Graphene based sensors and biosensors. *TrAC Trends in Analy. Chem.* **2017**, *91*, 53-66.

27. Liu, S.; Zeng, T.H.; Hofmann, M.; Burcombe, E.; Wei, J.; Jiang, R.; Kong, J.; Chen, Y. Antibacterial activity of graphite, graphite oxide, graphene oxide, and reduced graphene oxide: Membrane and oxidative stress. *ACS nano* **2011**, *5*, 6971-6980.
28. Xu, C.; Xu, B.; Gu, Y.; Xiong, Z.; Sun, J.; Zhao, X. Graphene-based electrodes for electrochemical energy storage. *Ener. Envi. Sci.* **2013**, *6*, 1388-1414.
29. Chen, Y.; Prasad, K.P.; Wang, X.; Pang, H.; Yan, R.; Than, A.; Chan-Park, M.B.; Chen, P. Enzymeless multi-sugar fuel cells with high power output based on 3d graphene–co 3 o 4 hybrid electrodes. *Phys. Chem. Chem. Phys.* **2013**, *15*, 9170-9176.
30. Lee, G.-H.; Cooper, R.C.; An, S.J.; Lee, S.; van der Zande, A.; Petrone, N.; Hammerberg, A.G.; Lee, C.; Crawford, B.; Oliver, W. High-strength chemical-vapor–deposited graphene and grain boundaries. *Science* **2013**, *340*, 1073-1076.
31. Muthoosamy, K.; G Bai, R.; Manickam, S. Graphene and graphene oxide as a docking station for modern drug delivery system. *Curr. Drug Deliv.* **2014**, *11*, 701-718.
32. Beyth, N.; Houri-Haddad, Y.; Domb, A.; Khan, W.; Hazan, R. Alternative antimicrobial approach: Nano-antimicrobial materials. *Evidence-based Compleme. Alterna. Med.* **2015**, *2015*.
33. Wei, L.; Lu, J.; Xu, H.; Patel, A.; Chen, Z.-S.; Chen, G. Silver nanoparticles: Synthesis, properties, and therapeutic applications. *Drug Disco. Today* **2015**, *20*, 595-601.
34. Tran, Q.H.; Le, A.-T. Silver nanoparticles: Synthesis, properties, toxicology, applications and perspectives. *Adv. Natu. Sci.: Nanosci. Nanotech.* **2013**, *4*, 033001.
35. Morones, J.R.; Elechiguerra, J.L.; Camacho, A.; Holt, K.; Kouri, J.B.; Ramírez, J.T.; Yacaman, M.J. The bactericidal effect of silver nanoparticles. *Nanotechnology* **2005**, *16*, 2346.
36. Rai, M.; Deshmukh, S.; Ingle, A.; Gade, A. Silver nanoparticles: The powerful nanoweapon against multidrug-resistant bacteria. *J. Appl. Microbio.* **2012**, *112*, 841-852.
37. Jung, W.K.; Koo, H.C.; Kim, K.W.; Shin, S.; Kim, S.H.; Park, Y.H. Antibacterial activity and mechanism of action of the silver ion in *staphylococcus aureus* and *escherichia coli*. *Appl. Envi. Microbio.* **2008**, *74*, 2171-2178.
38. Shao, W.; Liu, X.; Min, H.; Dong, G.; Feng, Q.; Zuo, S. Preparation, characterization, and antibacterial activity of silver nanoparticle-decorated graphene oxide nanocomposite. *ACS Appl. Mater. Interfaces* **2015**, *7*, 6966-6973.
39. Men, B.; Sun, Y.; Tang, Y.; Zhang, L.; Chen, Y.; Wan, P.; Pan, J. Highly dispersed ag-functionalized graphene electrocatalyst for oxygen reduction reaction in energy-saving electrolysis of sodium carbonate. *Indus. Eng. Chem. Res.* **2015**, *54*, 7415-7422.
40. Yu, L.; Zhang, Y.; Zhang, B.; Liu, J. Enhanced antibacterial activity of silver nanoparticles/halloysite nanotubes/graphene nanocomposites with sandwich-like structure. *Scient. Rep.* **2014**, *4*, 4551.
41. Xu, W.-P.; Zhang, L.-C.; Li, J.-P.; Lu, Y.; Li, H.-H.; Ma, Y.-N.; Wang, W.-D.; Yu, S.-H. Facile synthesis of silver@ graphene oxide nanocomposites and their enhanced antibacterial properties. *J. Mater. Chem.* **2011**, *21*, 4593-4597.
42. Al-Marri, A.H.; Khan, M.; Shaik, M.R.; Mohri, N.; Adil, S.F.; Kuniyil, M.; Alkhathlan, H.Z.; Al-Warthan, A.; Tremel, W.; Tahir, M.N. Green synthesis of pd@ graphene nanocomposite: Catalyst for the selective oxidation of alcohols. *Arabi. J. Chem.* **2016**, *9*, 835-845.
43. Iravani, S. Green synthesis of metal nanoparticles using plants. *Green Chem.* **2011**, *13*, 2638-2650.
44. Shaikh, A.; Parida, S.; Böhm, S. One step eco-friendly synthesis of ag–reduced graphene oxide nanocomposite by phytoreduction for sensitive nitrite determination. *RSC Adv.* **2016**, *6*, 100383-100391.

45. Muthoosamy, K.; Bai, R.G.; Abubakar, I.B.; Sudheer, S.M.; Lim, H.N.; Loh, H.-S.; Huang, N.M.; Chia, C.H.; Manickam, S. Exceedingly biocompatible and thin-layered reduced graphene oxide nanosheets using an eco-friendly mushroom extract strategy. *Int. J. Nanomed.* **2015**, *10*, 1505.

46. Kontogiannopoulos, K.N.; Assimopoulou, A.N.; Tsivintzelis, I.; Panayiotou, C.; Papageorgiou, V.P. Electrospun fiber mats containing shikonin and derivatives with potential biomedical applications. *Int. J. Pharmaceutics* **2011**, *409*, 216-228.

47. Cheng, M.-L.; Lin, C.-C.; Su, H.-L.; Chen, P.-Y.; Sun, Y.-M. Processing and characterization of electrospun poly (3-hydroxybutyrate-co-3-hydroxyhexanoate) nanofibrous membranes. *Polymer* **2008**, *49*, 546-553.

48. Schniepp, H.C.; Li, J.-L.; McAllister, M.J.; Sai, H.; Herrera-Alonso, M.; Adamson, D.H.; Prud'homme, R.K.; Car, R.; Saville, D.A.; Aksay, I.A. Functionalized single graphene sheets derived from splitting graphite oxide. *J. Phys. Chem. B* **2006**, *110*, 8535-8539.

49. Lian, P.; Zhu, X.; Liang, S.; Li, Z.; Yang, W.; Wang, H. Large reversible capacity of high quality graphene sheets as an anode material for lithium-ion batteries. *Electrochimica Acta* **2010**, *55*, 3909-3914.

50. Lukman, A.I.; Gong, B.; Marjo, C.E.; Roessner, U.; Harris, A.T. Facile synthesis, stabilization, and anti-bacterial performance of discrete ag nanoparticles using medicago sativa seed exudates. *J. Colli. Interface Sci.* **2011**, *353*, 433-444.

51. Gurunathan, S.; Han, J.W.; Dayem, A.A.; Eppakayala, V.; Kim, J.-H. Oxidative stress-mediated antibacterial activity of graphene oxide and reduced graphene oxide in pseudomonas aeruginosa. *Int. J. Nanomed.* **2012**, *7*, 5901.

52. Liu, K.; Zhang, J.-J.; Cheng, F.-F.; Zheng, T.-T.; Wang, C.; Zhu, J.-J. Green and facile synthesis of highly biocompatible graphene nanosheets and its application for cellular imaging and drug delivery. *J. Mater. Chem.* **2011**, *21*, 12034-12040.

53. Murdock, R.C.; Braydich-Stolle, L.; Schrand, A.M.; Schlager, J.J.; Hussain, S.M. Characterization of nanomaterial dispersion in solution prior to in vitro exposure using dynamic light scattering technique. *Toxico. Sci.* **2008**, *101*, 239-253.

54. Bykkam, S.; Rao, K.; Chakra, C.; Thunugunta, T. Synthesis and characterization of graphene oxide and its antimicrobial activity against klebseilla and staphylococus. *Int. J. Adv. Biotech. Res.* **2013**, *4*, 142-146.

55. Guo, H.-L.; Wang, X.-F.; Qian, Q.-Y.; Wang, F.-B.; Xia, X.-H. A green approach to the synthesis of graphene nanosheets. *ACS nano* **2009**, *3*, 2653-2659.

56. Han, J.W.; Gurunathan, S.; Jeong, J.-K.; Choi, Y.-J.; Kwon, D.-N.; Park, J.-K.; Kim, J.-H. Oxidative stress mediated cytotoxicity of biologically synthesized silver nanoparticles in human lung epithelial adenocarcinoma cell line. *Nanoscale Res. Lett.* **2014**, *9*, 459.

57. Salim, Y.S.; Chan, C.H.; Sudesh, K.; Gan, S.N. In *Influence of thermal treatment on the molecular weights of polyhydroxyalkanoate containing 3-hydroxyhexanoate*, *Adv. Mater. Res.*, **2013**; Trans Tech Publ: pp 250-253.

58. Shamala, T.; Divyashree, M.; Davis, R.; Kumari, K.S.L.; Vijayendra, S.V.; Raj, B. Production and characterization of bacterial polyhydroxyalkanoate copolymers and evaluation of their blends by fourier transform infrared spectroscopy and scanning electron microscopy. *Ind. J. Microbio.* **2009**, *49*, 251-258.

59. Hu, N.; Gao, R.; Wang, Y.; Wang, Y.; Chai, J.; Yang, Z.; Kong, E.S.-W.; Zhang, Y. The preparation and characterization of non-covalently functionalized graphene. *J. Nanosci. Nanotech.* **2012**, *12*, 99-104.

60. Choi, B.G.; Park, H.; Park, T.J.; Yang, M.H.; Kim, J.S.; Jang, S.-Y.; Heo, N.S.; Lee, S.Y.; Kong, J.; Hong, W.H. Solution chemistry of self-assembled graphene nanohybrids for high-performance flexible biosensors. *ACS nano* **2010**, *4*, 2910-2918.